Materials Research Bulletin 93 (2017) 170–176

Contents lists available at ScienceDirect

Materials Research Bulletin

journal homepage: www.elsevier.com/locate/matresbu

Effect of Yb^{3+} ions on structural and NIR emission of SrF_2:Eu^{2+}/Pr^{3+} down-conversion containing Na^+ ions

M.Y.A Yagoub[a,b], H.C. Swart[a], E. Coetsee[a,*]

[a] Department of Physics, University of the Free State, PO Box 339, Bloemfontein, ZA9300, South Africa
[b] Department of Physics, Sudan University of Science and Technology, Khartoum, Sudan

ARTICLE INFO

Article history:
Received 9 November 2016
Received in revised form 25 April 2017
Accepted 25 April 2017
Available online 26 April 2017

Keywords:
SrF_2
$NaYbF_4$
XPS
Yb oxidation states
Multiplet splitting

ABSTRACT

The influence of Yb^{3+} ions on the structural and near infra-red (NIR) emission of the SrF_2:Eu^{2+}/Pr^{3+} down-conversion containing Na^+ ions were investigated for solar cell applications. Most of the down-conversion studied materials for solar cell application are based on energy transfer from lanthanide ions to Yb^{3+} ions. For fluoride materials the charge compensation mechanism is of fundamental importance to maintain the electrical neutrality of the crystals. The x-ray diffraction data indicated that a mixture of cubic SrF_2 and $NaYbF_4$ phases gradually formed with increasing Yb^{3+} doping concentration. X-ray photoelectron spectroscopy (XPS) also confirmed the formation of the mixed fluoride structures. The F 1*s* peak showed two peaks that were assigned to SrF_2 and $NaYbF_4$. A negligible amount of Yb^{3+} ions that were converted into Yb^{2+} ions was also detected with XPS. From the photoluminescence data it was evident that the Na^+ ions induced noticeable change to the NIR emission. This might reduce the quantum efficiency between the Pr^{3+} and Yb^{3+} ions in the system.

1. Introduction

Down-conversion materials with quantum effects are luminescent nanomaterials that convert one high energy photon into two lower energy photons through lanthanide doping [1–4]. The quantum cutting was observed in Pr^{3+} singly doped fluoride materials where the quantum cutting emission was detected in the visible region [5]. Recently the visible quantum cutting with high efficiency has also been demonstrated in other lanthanide ions [6]. Nowadays, most attention has been given towards down-conversion for enhancing the efficiency of solar cells through doping fluoride materials with lanthanide ions (Ln^{3+}) [2,4]. Most of the down-conversion studied materials, however, are based on the energy transfer from Ln^{3+} (activators) to Yb^{3+} ions [1,2,4]. Intense UC and DC emissions were observed when $Gd_2(WO_4)_3$: Er^{3+}/Yb^{3+} phosphors were excited at 980 nm and 380 nm, and different pumping mechanisms and different depopulation routes were considered to be responsible for the different concentration quenching behaviours [7]. Selectively enhanced green UC and near-infrared (NIR) DC emissions of Er^{3+} by Yb^{3+}-Mn^{2+} dimer sensitizing have been demonstrated in Er^{3+}/Yb^{3+}/Mn^{2+} tri-doped spinel $MgGa_2O_4$ upon excitation with a 980 nm laser diode [8]. $CaLaNb_3O_{10}$:Yb^{3+} micro-particles were synthesised by the convenient solid-state reaction method. The phosphors presented a broad absorption band in the UV region below 350 nm. The down-conversion from UV light to the NIR band at 910–1100 nm due to the $^2F_{5/2}$-$^2F_{7/2}$ transition in Yb^{3+}-doped $CaLaNb_3O_{10}$ is reported. The luminescence properties confirm the occurrence of energy transfer from niobate groups to Yb^{3+} ions in the lattices [9]. SrF_2: Pr^{3+}-Yb^{3+} down-conversion couple was reported as one of the best quantum cutting couples [4]. It consists of a two-step resonance energy transfer process. The two-step resonance energy transfer process between Pr^{3+} and Yb^{3+} with the $^1G_4$ level of Pr^{3+} acting as the intermediate level occur through Pr^{3+}: [$^3P_0$-$^1G_4$, $^1G_4$-$^3H_4$] → 2 × Yb^{3+}: [$^2F_{7/2}$-$^2F_{5/2}$]. This gave rise to emission of two near infrared photons with a quantum efficiency close to 200%. The charge compensation in fluoride hosts plays a crucial role in the down-conversion process [1,4,10,11]. The extra charge of Ln^{3+} is locally compensated by F^- ions. A new class of charge compensation based on monovalent impurity ions (such as Na^+) also exist along with trivalent lanthanide ions (Ln^{3+}) into fluorite hosts [12–14]. Co-doping Yb^{3+} with Na^+ as a charge compensator decreases the multisites of Yb^{3+} since Yb^{3+}-Na^+ complexes are expected to dominate the system [12].

However, a prime limitation in the use of the down-conversion couples, such as Pr^{3+}-Yb^{3+} ions, in solar cell application is its 4f-4f absorption cross-section. The forbidden 4f-4f transitions of the Pr^3

* Corresponding author.
E-mail addresses: CoetseeE@ufs.ac.za, swarthc@ufs.ac.za (E. Coetsee).

http://dx.doi.org/10.1016/j.materresbull.2017.04.049
0025-5408/

$^{+}$ ion is characterized by a low absorption cross-section [1]. A suggestion to this limitation is to add a third sensitizer with dipole-allowed 4f–5d transitions, such as Ce^{3+}, Eu^{2+} and Yb^{2+} [1,13,15–19]. Eu^{2+} ions greatly enhanced the visible emission of the Pr^{3+} in SrF_2 with Na^{+} ions as charge compensator [20]. It is therefore quite meaningful to investigate the effect of Eu^{2+} on the near infra-red (NIR) emission of the Pr^{3+}-Yb^{3+} couple in a SrF_2 crystal for solar cell application. In this study we reported on the processing conditions of Yb^{3+} doped SrF_2:Eu^{2+}/Pr^{3+} containing Na^{+} ions. Some aspects of their dependence on structural, compositional and NIR photo-luminescence (PL) properties as a function of Yb^{3+} dopant concentration are discussed.

2. Experimental

The phosphor samples were synthesised by the co-precipitation method. Analytical grade of $Sr(NO_3)_2$, $Eu(NO_3)_3{\cdot}5H_2O$, $Yb(NO_3)_3{\cdot}5H_2O$ and NH_4F were used without further purification. For a typical synthesis of singly and co-doped SrF_2:Eu^{2+}/Pr^{3+} (1.5/2 mol %), xYb^{3+} (x = 0.5, 1, 3, 5, 7, 10, 15, 20, 30 mol%) and SrF_2: 1.5 mol%Eu^{2+}, xYb^{3+} (x = 1, 3, 5, 7, 10, 15, 20, 30, 40, 60 mol%), 30 mmol of NH_4F and 0.1 mol/mL of sodium hydroxide (Na^{+} source) were added drop-wise to an aqueous solution containing $Sr(NO_3)_2$, $Pr(NO_3)_3{\cdot}6H_2O$, $Yb(NO_3)_3{\cdot}5H_2O$ and $Eu(NO_3)_3{\cdot}5H_2O$ in a period of about 30 min. After one hour of stirring, the mixture was left for 5 h. Then, the product was collected by using a centrifugal and washed with water and ethanol. Finally, the product was dried for 48 h in an oven at 80 °C. The samples were annealed under a reducing atmosphere (Ar 96%/H_2 4%) in order to reduce Eu^{3+} into Eu^{2+} ions.

The structure of the prepared samples was characterized by X-ray diffraction (XRD) using a Bruker Advance D8 diffractometer (40 kV, 40 mA) with Cu K_α x-rays (λ = 0.154 nm). The morphology of the materials was analysed using a JEOL JSM-7800F high field emission scanning electron microscope (FE-SEM). High resolution x-ray photoelectron spectroscopy (XPS) spectra were obtained with a PHI 5000 Versaprobe system. A low energy Ar^{+} ion gun and low energy neutralizer electron gun were used to minimize charging on the surface. A 100 μm diameter monochromatic Al Kα x-ray beam ($h\nu$ = 1486.6 eV) generated by a 25 W, 15 kV electron beam was used to analyze the different binding energy peaks. The pass energy was set to 11 eV giving an analyzer resolution of ≤ 0.5 eV. Multipack version 8.2 software was utilized to analyze the spectra to identify the chemical compounds and their electronic states using Gaussian–Lorentz fits. The NIR PL spectra were collected with a He-Cd laser PL system with a 325 nm excitation wavelength and 2 mm InGaAs photodiode detector. All measurements were performed at room temperature.

3. Results and discussion

The XRD patterns of SrF_2:Eu^{2+}/Pr^{3+} (1.5/2 mol%) with different Yb^{3+} concentrations containing 0.5 mol% Na^{+} are shown in Fig. 1(a). For SrF_2:1.5 mol% Eu^{2+} and up to 15 mol% Pr^{3+}, the pattern

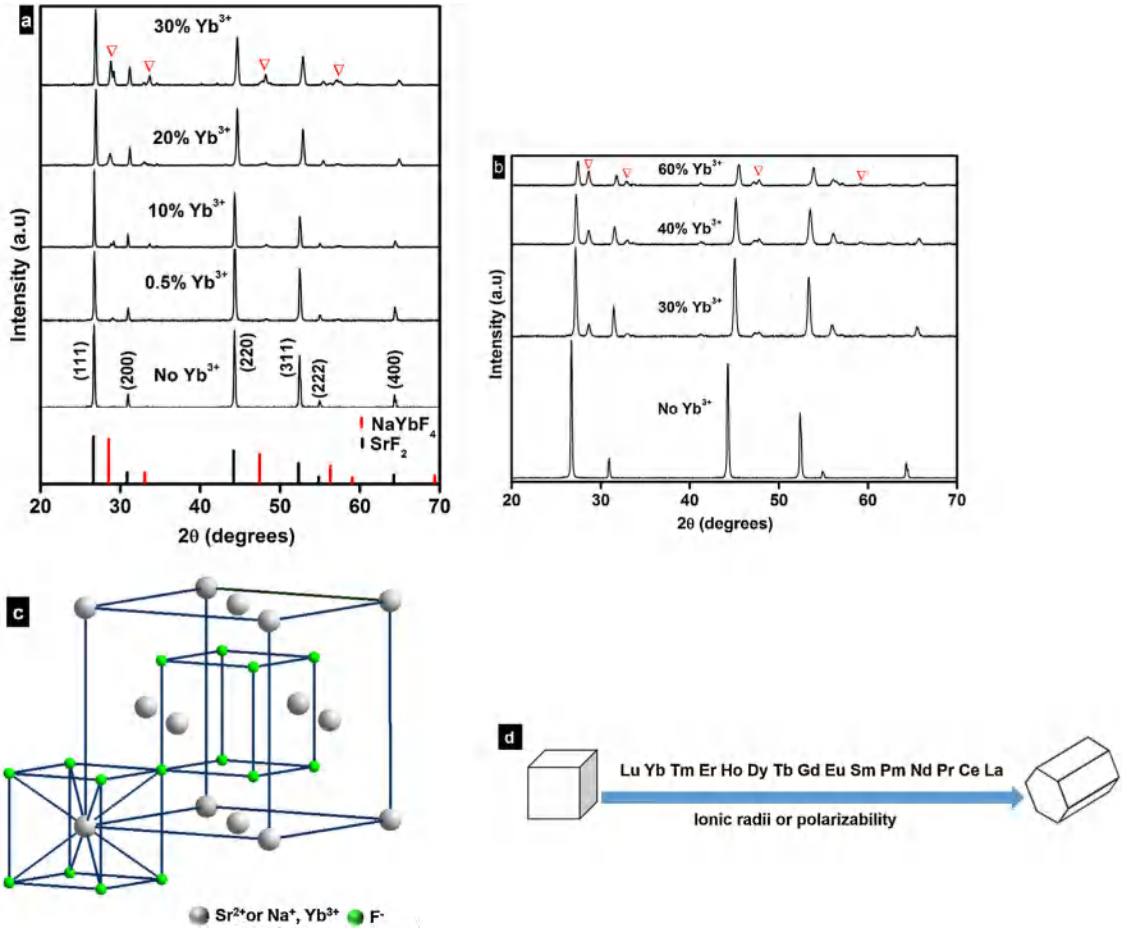

Fig. 1. X-ray diffraction patterns of (a) SrF_2:Eu^{2+}/Pr^{3+} (1.5/2 mol%) crystals and (b) SrF_2:Eu^{2+} (1.5 mol%) obtained after co-doping with different Yb^{3+} concentration and fixed 0.5 mol% Na^{+}. The peaks marked with a triangle refer to cubic-phase of $NaYbF_4$. (c) Schematic presentation of cubic phase of SrF_2 and $NaYbF_4$ structure. Showing each second simple cubic of F^{-} sublattice contains a Sr^{2+} ion and the other are empty. (d) General trend of the formation of cubic and hexagonal structures of sodium lanthanide fluoride as a function of lanthanide dopant ions.

crystallized into the cubic structure of SrF_2 (file number 00-086-2418). It can clearly be seen from the XRD pattern that doping with Yb^{3+} ions induced noticeable changes in the structural properties of the powder. Only a small amount of Yb^{3+} (0.5 mol%) ions incorporated into SrF_2:Eu^{2+}/Pr^{3+} (1.5/2 mol%) resulted in a mixture of the cubic SrF_2 and $NaYbF_4$ (JCPDS file number 77-2043) phases. The $NaYbF_4$ crystal systematically grown as the Yb^{3+} ions increased (see Fig. 1(a)). To confirm that doping with Yb^{3+} and Na^+ ions in the SrF_2 crystal induce structural changes on the SrF_2 powder, a series of SrF_2:Eu^{2+} (1.5 mol%), Na^+ (0.5%) co-doped with different Yb^{3+} ions were also investigated, as shown in Fig. 1(b). Here the mixture of the cubic SrF_2 and $NaYbF_4$ crystals formed at relatively high Yb^{3+} concentrations. The $NaYbF_4$ crystal was also grown with increasing Yb^{3+} concentrations. This result can therefore be attributed to the fact that the cubic $NaYbF_4$ system is a fluorite structure (SrF_2) with the Sr^{2+} sites randomly occupied by Na^+ and Yb^{3+} ions (Fig. 1(c)) [18]. They adapt the same space group (Fm-3m) (225). Importantly, lanthanide ions with small ionic radii favour the cubic structure of sodium lanthanide fluoride systems, while lanthanide ions with large ionic radii possess a high tendency towards electron cloud distortion owing to increase dipole polarizability and thus favour the hexagonal structure (Fig. 1(d)) [21]. This might be the reason why high Pr^{3+} concentrations could not cause noticeable structural changes in the SrF_2 system due to its tendency to form a hexagonal phase of the sodium lanthanide fluoride nanocrystal. Thus, the presence of Na^+ with increased Yb^{3+} concentration in the SrF_2 structure gradually lead to the formation of a mixture of cubic structures of SrF_2 and $NaYbF_4$. The peaks were shifted towards higher diffraction angles in the XRD patterns in Fig. 1 as a function of Yb^{3+} concentration. This is due to the Sr^{2+} substitution with Yb^{3+} ions in the host. From the XRD patterns of both the samples (a) and (b), Fig. 1, the cubic phase of the $NaYbF_4$ structure was observed at 0.5 mol% Yb^{3+} concentration in the SrF_2:Eu^{2+}/Pr^{3+} (1.5/2 mol%) sample compared to SrF_2: 1.5 mol% Eu^{2+}, which can be attributed to the lanthanide doping ions charge difference between the two samples.

SEM images were obtained in order to investigate the surface morphology of the phosphors. Fig. 2 shows the SEM image of 10 mol% Yb^{3+} triply doped SrF_2:Eu^{2+}/Pr^{3+} (1.5/2 mol%) containing 0.5 mol% Na^+. The image reveals that the powder consisted of agglomerated spherical particles with a diameter bigger than 100 nm. This agreed with our previous results on Eu^{2+} and Pr^{3+} co-doped SrF_2 [20], which confirmed that Yb^{3+} didn't change the morphology of the system.

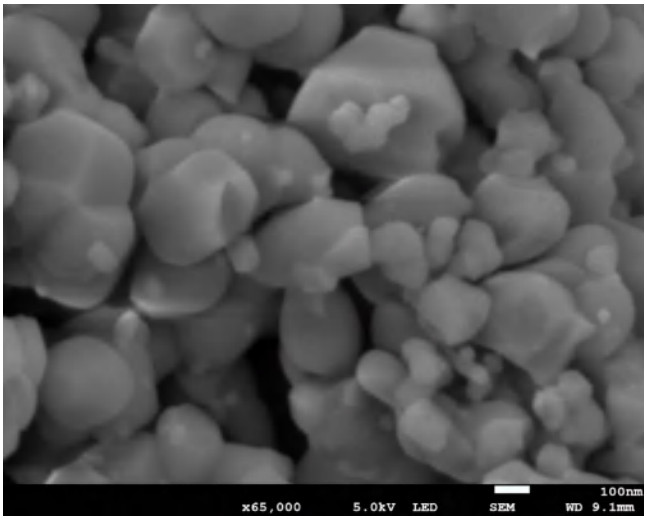

Fig. 2. SEM image of SrF_2:Eu,Pr,Yb phosphor powder.

We further studied the formation of the mixture structure of SrF_2 and $NaYbF_4$ of the samples using XPS. The insert graph of Fig. 3 shows the peak fit of the F 1*s* peak of the sample without Yb^{3+} ions. The peak consists of only one peak which can be assigned to the F 1*s* (684.7 eV) in the SrF_2 structure. Fig. 3(a) and (b) shows the peak fits for F 1*s* of the samples co-doped with Yb^{3+} ions (a) SrF_2:Eu^{2+}/Pr^{3+}, Yb^{3+} (1.5/2, 30 mol%) and (b) SrF_2:Eu^{2+}/Yb^{3+} (1.5/30 mol%) containing 0.5 mol% Na^+. During the peaks fit procedure, the C 1*s* peak at 284.8 eV was taken as a reference for all charge shift corrections [22]. In addition to that, all the Gaussian percentages were assumed to have a combined Gaussian-Lorentzian shape. The fit of the F 1*s* high resolution XPS peak for both the samples (a) and (b) showed two individual peaks. These two peaks are assigned to F 1*s* in SrF_2 and F 1*s* (685.9 eV) in $NaYbF_4$ structures, respectively. The peak position of the F 1*s* of both the components is found to be consistent in both the samples. It can be seen that from Fig. 3 the F 1*s* intensity of the SrF_2:Eu^{2+}/Yb^{3+} (1.5/30 mol%) is lower than that of the SrF_2:Eu^{2+}/Pr^{3+}, Yb^{3+} (1.5/2, 30 mol%). This is in a good agreement with the XRD results, where the $NaYbF_4$ structure formed at a low Yb^{3+} concentration in SrF_2:Eu^{2+}/Pr^{3+}, Yb^{3+} compared to the SrF_2:Eu^{2+}/Yb^{3+} system. On the other hand, Eu can occur in the divalent (Eu^{2+}) and in the trivalent (Eu^{3+}) states, while Pr can also occur in the trivalent (Pr^{3+}) and tetravalent (Pr^{4+}) states. Both the oxidation states of Eu are optically active and were detected in the SrF_2 host in our previous investigation [23]. Therefore, all the samples were annealed under a reducing

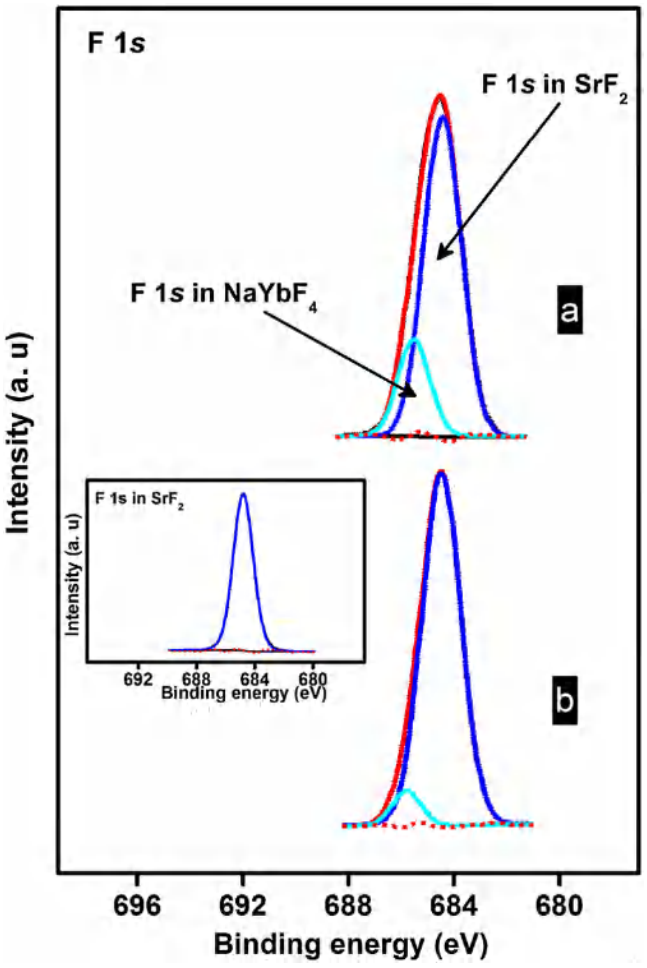

Fig. 3. High resolution XPS peaks of (a) SrF_2:Eu^{2+}/Pr^{3+}, Yb^{3+} (1.5/2, 30 mol%) and (b) SrF_2:Eu^{2+}/Yb^{3+} (1.5/30 mol%) phosphors powder containing 0.5 mol% Na^+. The insert graph shows the F 1*s* peak of the SrF_2:Eu^{2+}/Pr^{3+} (1.5/4 mol%) without Yb^{3+} ions.

atmosphere (Ar 96%/H_2 4%) in order to reduce Eu^{3+} into Eu^{2+} ions. In our previous XPS investigation of SrF_2:Eu, Pr^{3+} phosphors powders the conversion process of Eu^{3+} to Eu^{2+} and the existence of only Pr^{3+} oxidation state were confirmed [20].

The Yb 4*d* spectrum of the SrF_2:Eu^{2+}/Pr^{3+}, Yb^{3+} (1.5/2, 30 mol%) sample is shown in Fig. 4. There was no difference observed in the XPS spectra of the two samples SrF_2:Eu^{2+}/Pr^{3+}, Yb^{3+} (1.5/2, 30 mol %) and SrF_2:Eu^{2+}/Yb^{3+} (1.5/30 mol%). The spectrum consists of mixed valence compounds of Yb ions (Yb^{3+} and Yb^{2+}). The conversion of a negligible amount of the Yb^{3+} to Yb^{2+} under H_2 atmosphere at high temperature was also realized in a study done on a CaF_2 crystal [24]. The 4*f* states of Yb^{2+} are completely filled with electrons, therefore, exchange interaction between a core hole and 4*f* electrons is negligibly small [25]. Hence, the 4*d* spectrum of the Yb^{2+} exhibits only the two peaks that arise from the spin-orbit splitting. A small shoulder *a*' located at 181.5 eV and a peak *b*' at 190.4 eV are assigned to the $4d_{5/2}$ and $4d_{3/2}$ components of Yb^{2+}, respectively. The spin-orbit splitting value is 8.9 eV, and it is in a good agreement with the reported value [25]. On the other hand, it can clearly be seen that the other peaks (labelled a, b, c, d, e and f) contradict the 3/2 intensity ratio expected when spin-orbit splitting is present. Therefore, these peaks are associated with the Yb^{3+} $4d_{5/2}$ multiplet splitting due to the interaction with the 4f energy level, rather than spin-orbit splitting. LS coupling divides the final state of $4d^9 4f^{13}$ into the ^{3}(HGFDP) and ^{1}(HGFDP) states [25,26]. The XPS peak positions, area distributions and FWHM of the Yb 4*d* peak are tabulated in Table 1.

The visible emission of the SrF_2:Eu^{2+}/Yb (1.5/5 mol%) containing Na^+ ions excited by 325 nm is shown in Fig. 5. Under 325 nm excitation the PL spectrum consists of emission from only the Eu^{2+} ions. The strong broad emission band centred at 416 nm was assigned to the inter-configuration $4f^6 5d^1$-$4f^7$ allowed transition of Eu^{2+} [23,27]. The emission intensity variation of the Eu^{2+} as a function of Eu^{2+} concentration was investigated in a previous study [20]. The maximum luminescence intensity for Eu^{2+} singly doped has occurred for the sample doped with 1.5 mol% Eu^{2+}. The effect of the sensitizer ion concentrations on the acceptor emission has also been studied [28]. The concentration of maximum enhancement of the acceptor emission was found to be the same as the concentration for the maximum sensitizer emission intensity for the single doped samples. In this study there is no sign of Yb^{2+} emission in the visible region [24], which confirm that the concentration of Yb^{2+} in the sample has no influence in the PL emission in this study. It is worth noting that the emission band of Eu^{2+} overlaps with the excitation band of the ^3P_j (j = 0, 1, 2) Pr^{3+} ion, inset of Fig. 5(a). Fig. 5(b) portrays a comparison between the PL spectra of the SrF_2:Eu^{2+} (1.5 mol%), Pr^{3+} (0.3 mol%) and 0.3 mol% Pr^{3+} singly doped in SrF_2 excited by 332 and 439 nm, respectively. The emission bands of Pr^{3+} in SrF_2 were clearly observed in both

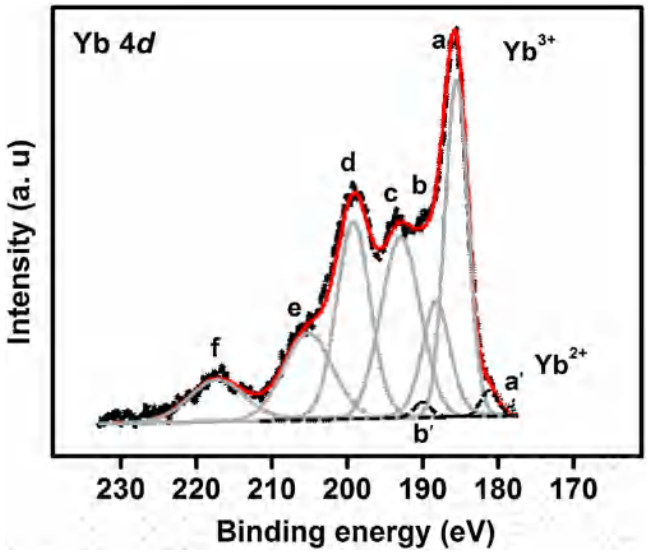

Fig. 4. Yb 4*d* spectrum of SrF_2:Eu^{2+}/Pr^{3+}, Yb^{3+} (1.5/2, 30 mol%) sample. Solid and dotted lines represent Yb^{3+} and Yb^{2+} components, respectively.

Table 1
XPS peak position, FWHM and area distribution of the Yb 4*d* peak of the SrF_2:Eu^{2+}/Pr^{3+}, Yb^{3+} (1.5/2, 30 mol%) phosphor powder.

Peak label	B.E (±0.1 eV)	FWHM (eV)	Area distribution
a	181.5	2.67	215
b	190.4	2.67	142
a	185.9	3.69	3910
b	188.6	4.32	1739
c	193.4	6.23	3543
d	199.7	5.30	3437
e	205.7	7.72	2212
f	217.8	8.72	1191

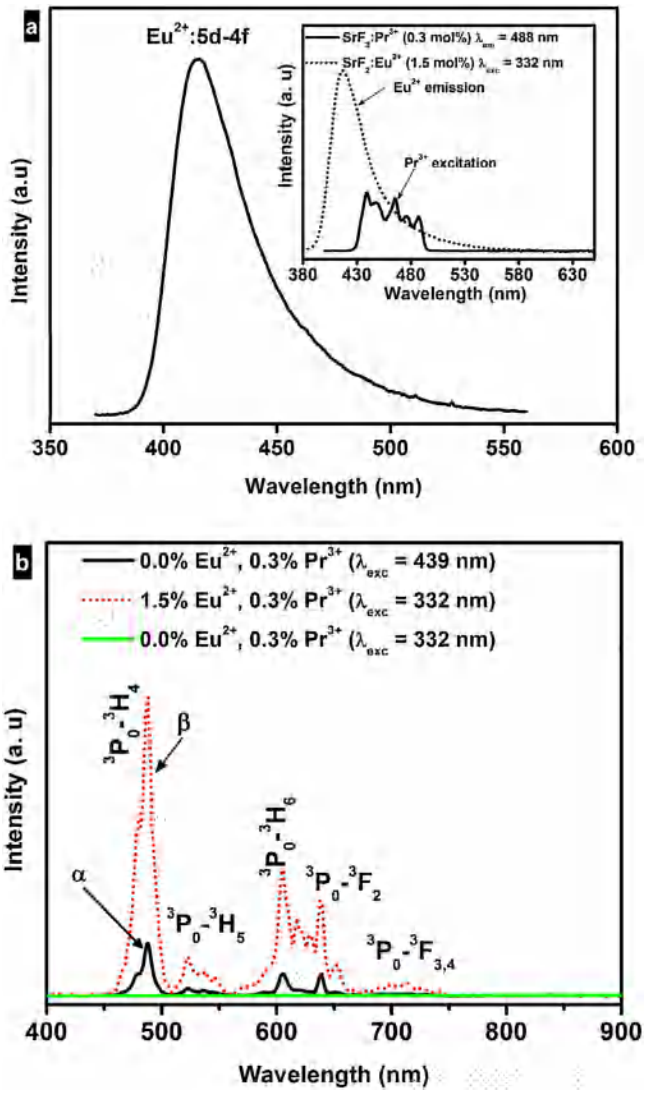

Fig. 5. (a) visible emission of the SrF_2:Eu^{2+}/Yb (1.5/5 mol%) containing 0.5 mol% Na^+ ions excited by the He-Cd laser system with 325 nm excitation wavelength. Inset is spectral overlap between Eu^{2+} emission and Pr^{3+} excitation in the SrF_2 crystal structure. (b) a comparison between Pr^{3+} singly doped (??) and Eu^{2+} co-doped (??) ions in SrF_2 containing 0.5 mol% Na^+.

spectra. All the Pr^{3+} emission bands were significantly enhanced in the co-doped sample. The biggest enhancement is for the 488 nm band ($^3P_0 \rightarrow {}^3H_4$ transition). A comparison between the total calculated intensity emissions revealed that the Pr bands in the co-doped sample have been enhanced by nearly six times. Fig. 5(b) also includes the emission spectrum of the $SrF_2:Pr^{3+}$ (0.3 mol%) without Eu^{2+} excited at 332 nm. It clearly shows that Eu^{2+} well enhanced the emission of Pr^{3+} in the co-doped sample. The detailed energy transfer between Eu^{2+} and Pr^{3+} in SrF_2 containing Na^+ ions was previously investigated where the Pr^{3+} ions induced faster decay to Eu^{2+} lifetime [20].

The PL spectra of the NIR region are shown in Fig. 6. Fig. 6(a) portrays NIR emission of the $SrF_2:Eu^{2+}/Pr^{3+}$ (1.5/2 mol%) 0.5 mol% Na^+ containing sample with different Yb concentrations upon Eu^{2+} excitation. For the sample co-doped with only Eu^{2+} (1.5 mol%) and Pr^{3+} (2 mol%) (Shown in Fig. 6(a) as 0.0% Yb), a number of NIR bands can be observed. The emission band centred at 993 nm with small shoulders at 1004 and 1015 nm is ascribed to the transition of the lowest stark level of $^1G_4$ in Pr^{3+} to different Stark levels of the $^3H_4$ level [14]. The other peaks located at 1057, 1080 and 1307 nm are assigned to the transitions of $^1D_2$-$^3F_3$, $^1D_2$-$^3F_4$ and $^1G_4$-$^3H_5$ in Pr^{3+}, respectively. The observation of emission bands originating from the $^1D_2$ level implies that cross-relaxation between the Pr^{3+} ions pairs occurred in NIR region since the multi-phonon relaxation process from $^3P_0$ to $^1D_2$ level is negligible in a fluoride crystal [29]. After doping with Yb^{3+} ions a sharp and small PL peak appears at 977 nm, which is attributed to the 4f–4f transition of Yb^{3+}:$^3F_{5/2}$-$^3F_{7/2}$ [4]. At 10 mol% Yb^{3+}, the NIR emission of Pr^{3+} is almost completely quenched and the Yb^{3+} emission clearly observed. A comparison between the NIR emission of the $SrF_2:Eu^{2+}/Pr^{3+}$, Yb^{3+} (1.5/2, 10 mol %) containing 0.5 mol% Na^+ ions and $SrF_2:Eu^{2+}/Pr^{3+}$, Yb^{3+} (1.5/2, 10 mol%) without Na^+ ions is also shown in Fig. 6(b) where there is no emission from the Pr^{3+} peak observed in the spectrum without Na^+ ions. The emission of Yb^{3+} in the sample containing Na^+ ions was characterized by a weak intensity compared to that without Na^+ ions. In the emission spectrum of the material that contained 0.5 mol% Na^+ ions some of the Pr^{3+} emission peaks was also detected (Fig. 6(b)). Furthermore, the emission intensity of the sample with Na^+ ions was much weaker compared to that without the 0.5 mol% Na^+. The Yb^{3+} emission in this results that contained 0.5 mol% Na^+ ions is also in contrast with results obtained in Ref. [4]. In ref [4], efficient energy transfer between Pr^{3+} and Yb^{3+} occurred and strong emission of Yb^{3+} and no emission from Pr^{3+} in the NIR region were observed at such concentrations. From these results someone can notice that the presence of Na^+ ions led the Pr^{3+} ions to emit in the NIR region, which suppressed the NIR emission of the Yb^{3+} ions. Furthermore, from this result and Ref. [4] we can conclude that the presence of Na^+ ions in the system containing Pr^{3+} and Yb^{3+} ions reduced the energy transfer efficiency between Pr^{3+} and Yb^{3+}.

The NIR emission spectra of the Yb^{3+} co-doped in the $SrF_2:Eu^{2+}$ are shown in Fig. 6(c). The emission is characteristic of the Yb^{3+} ion transitions from the excited state $^2F_{5/2}$ to the ground state $^2F_{7/2}$ [1,2,4]. The Yb^{3+} emission through Eu^{2+} excitation has been reported to occur through cooperative quantum cutting energy transfer [30–32]. One can see that the emission intensity of Yb^{3+} at 1 mol% (Fig. 6(c)) is relatively different from the other spectra. It consists of two narrow peaks centered at 978 and 1035 nm. With increased Yb^{3+} concentration, the shape and position of these two peaks were significantly changed. The peak at 1035 nm strongly blue shifted whereas the peaks at 978 nm gradually blue shifted and broaden. The emission of Yb^{3+} ions as function of doping concentrations without Na^+ ions has been previously reported where there was no shift in the Yb^{3+} peak position observed [33]. This result suggested that the Yb^{3+} emission was affected by the Na^+ impurity ions. The influence of Na^+ ion concentrations on the

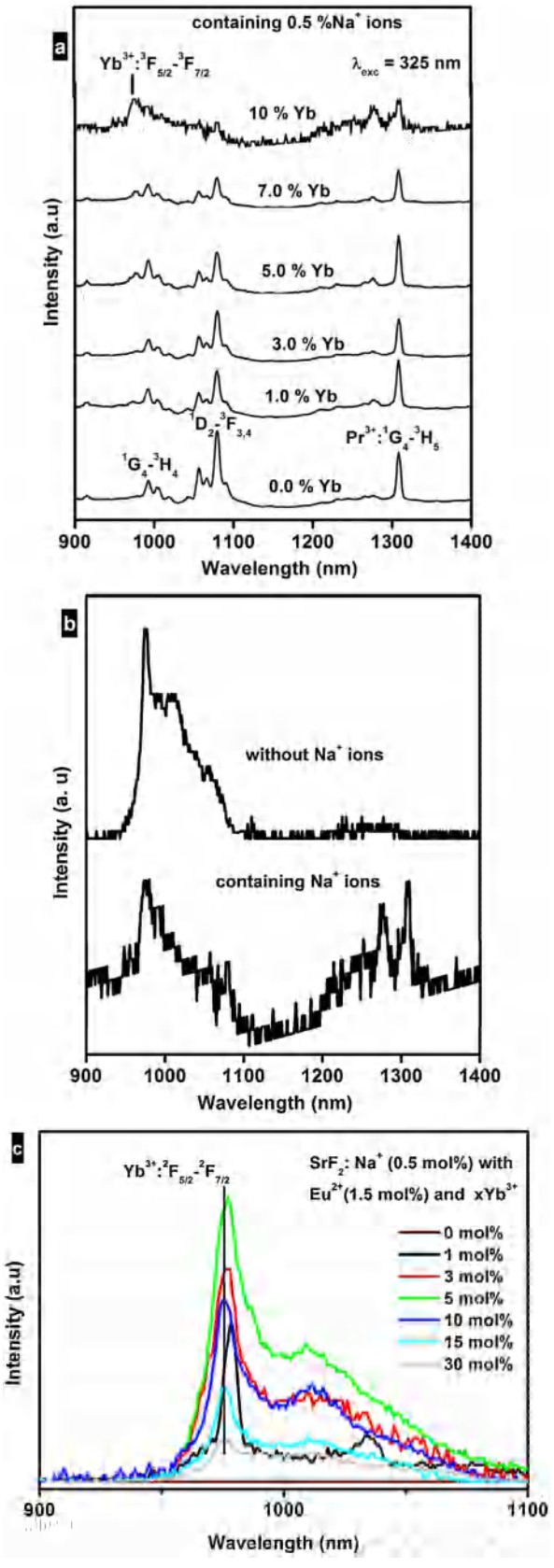

Fig. 6. NIR emission spectra of (a) $SrF_2:Eu^{2+}/Pr^{3+}$, Yb^{3+} (1.5/2 mol%) with different Yb^{3+} concentration; (b) A comparison between $SrF_2:Eu^{2+}/Pr^{3+}$, Yb^{3+} (1.5/2, 10 mol%) containing 0.5% Na^+ ions and $SrF_2:Eu^{2+}/Pr^{3+}$, Yb^{3+} (1.5/2, 10 mol%) without Na^+ ions; and (c) $SrF_2:Eu^{2+}$ (1.5 mol%) as a function of Yb^{3+} concentration excited by the He-Cd laser system with 325 nm excitation wavelength.

absorption and emission of the Yb^{3+} ions singly doped fluoride materials has been previously reported [12,14]. All these previous studies agreed that the Na^{+} ions resulted in narrow and clearly resolved, with small blue shifted, emission and absorption spectra of the Yb^{3+} ions. In this study, one can conclude that the Na^{+} impurity ions influenced the Yb^{3+} spectra at low Yb^{3+} concentration. This is because at low Yb^{3+} concentration the Na^{+} sites are abundant whereas with increasing Yb^{3+} concentration the structure gradually transformed to a mixture of cubic phases of SrF_2 and $NaYbF_4$ structures [34].

The luminescence decay curves of Eu^{2+} singly and co-activated SrF_2 with Pr^{3+} or Pr^{3+}-Yb^{3+} as well as Yb^{3+} are shown in Fig. 7. The decay time for the singly doped Eu^{2+} was 435 ns (Fig. 7A). This decay time was due to radiative decay from the $4f^{6}5d^{1}$ (T_{2g}) level, which is in agreement with reported values for the decay time of Eu^{2+} emission in SrF_2 [29]. Co-doping with 2 mol% of Pr^{3+} induced faster decay, which can be attributed to the energy transfer from Eu^{2+} to Pr^{3+}, Fig. 7(C). Adding 1 mol% of Yb^{3+} to the Eu^{2+}-Pr^{3+} couple dramatically decreased the Eu^{2+} decay lifetime, Fig. 7(D). The decay curve of Eu^{2+}-Yb^{3+} is also shown in Fig. 7(B). The bi-exponential decay curve of 1.5 mol%Eu^{2+} and 1 mol%Yb^{3+} indicates that energy transfer from Eu^{2+} to Yb^{3+} occurred. The decay curve of Eu^{2+} in SrF_2:Eu^{2+}-Yb^{3+} system was previously studied where the lifetime of Eu^{2+} was strongly affected by the presence of Yb^{3+} [28]. However, There is a fast decay curve in the Pr^{3+} curve with increasing Yb^{3+} concentration in SrF_2:Eu^{2+},Pr^{3+}-Yb^{3+} system. At high Yb^{3+} concentrations, the decay curves however seem to remain constant. This might be attributed to the decrease in the Pr^{3+} lifetime towards nanoseconds and this exceeded the pulsed duration of the YAG laser system (in microseconds), which was used to measure the Pr^{3+} PL decay curves.

It is observed from both Figs. 6(a) and (c) that the NIR PL intensity drastically drops for the highest concentration of Yb^{3+}. This can be attributed to the concentration luminescent quenching due to the formation of clusters among Yb^{3+} ions. In the SrF_2:Eu^{2+}/Pr^{3+}, Yb^{3+} sample the relatively weak emission of Yb^{3+} at low Yb^{3+} concentration may be due to the strong emission of the Pr^{3+}:4f-4f bands that overlaps with Yb^{3+} emission. The strong emission of Pr^{3+} in the NIR region in this study is due to the presence of the Na^{+} ions in the system. The schematic diagram of the possible NIR emission in the system is sketched in Fig. 8. The NIR emission is a combination of both ions, Pr^{3+} and Yb^{3+}. Fig. 8 illustrates that the NIR emission of Yb^{3+} in SrF_2:Eu^{2+},Pr^{3+}-Yb^{3+} might be as a result of a cooperative energy transfer from Eu^{2+} (Fig. 8(II)) or a single-energy

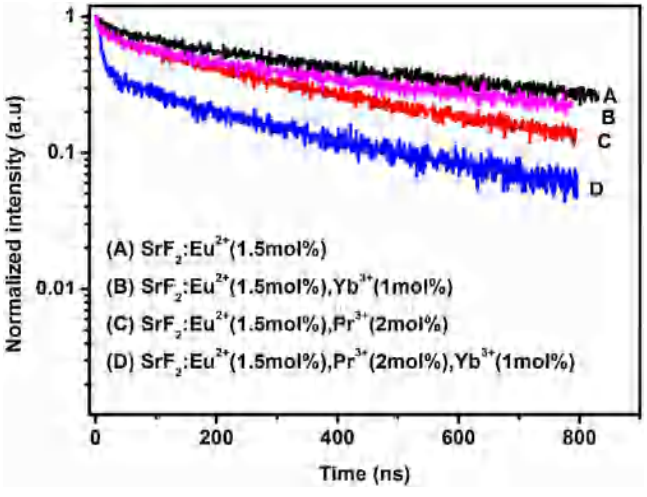

Fig. 7. Decay curve of Eu^{2+} co-activated Pr^{3+} and Yb^{3+} in SrF_2 contains 0.54 mol% of Na^{+}.

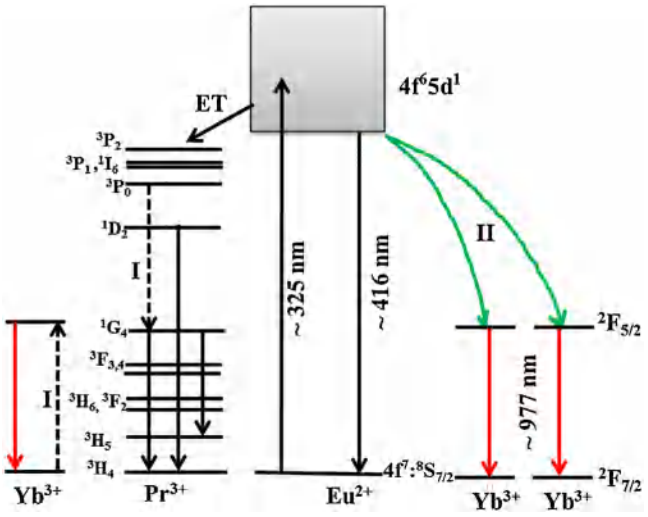

Fig. 8. (Color online) schematic diagram energy level and down-conversion mechanism for the Eu^{2+} sensitized Pr^{3+}, Yb^{3+} couple. The diagram shows the cooperative energy transfer and single-energy transfer between Eu^{2+} and Pr^{3+} to Yb^{3+} respectively.

transfer from Pr^{3+} ion or a combination of both Eu^{2+} and Pr^{3+} to Yb^{3+} ion. In a single-energy transfer from Pr^{3+} to Yb^{3+} process, illustrated in Fig. 8(I), the energy transfer occurred as fellow: Pr^{3+}:($^{3}P_0$-$^{1}G_4$)-Yb^{3+}:($^{2}F_{5/2}$-$^{2}F_{7/2}$). Since the cooperative energy transfer is second-order and Yb^{3+} gives a weak emission intensity one can suggest that the single-energy transfer between Pr^{3+} and Yb^{3+} ion might occurred in the presence of Na^{+} ions in the system. However, from this study a small amount of Na^{+} ions (only 0.5 mol%) as charge compensation in the Yb^{3+} triply doped SrF_2:Eu^{2+},Pr^{3+} system has noticeable effect on the NIR emission of both Pr^{3+} and Yb^{3+} ions. It means that using Na^{+} ions as charge compensation in a quantum cutting process with Pr^{3+} and Yb^{3+} is essential and must be taken into account.

4. Conclusion

The powder samples in this work were prepared by the co-precipitation method to study the influence of Yb^{3+} doping concentration on the structural and NIR photoluminescence properties of SrF_2:Eu^{2+}/Pr^{3+} down-conversion containing Na^{+} ions. XRD results showed a mixture of the cubic phases of SrF_2 and $NaYbF_4$ with increasing Yb^{3+} concentration. The formation of the mix fluoride structure was also confirmed by XPS where the F 1*s* high resolution peak showed two peaks assigned to SrF_2 and $NaYbF_4$. Although a negligible amount of Yb^{3+} ions were converted into Yb^{2+} there was no emission peaks of Yb^{2+} observed. From the photoluminescence data it was evident that Na^{+} induced significant changes to the NIR emission. Pr^{3+} strongly emitted in the NIR region that suppressed the Yb^{3+} emission. This reduced the energy transfer efficiency between Pr^{3+} and Yb^{3+} in the system.

Acknowledgments

This work is based on the research supported by the South African Research Chairs Initiative of the Department of Science and Technology (84415) and National Research Foundation of South Africa. The financial assistance of the National Research Foundation (NRF) and the University of the Free State towards this research is hereby acknowledged.

References

[1] B.M. Van der Ende, L. Aarts, A. Meijerink, Phys. Chem. Chem. Phys. 11 (2009) 11081–11095.
[2] X. Huang, S. Han, W. Huang, X. Liu, Chem. Soc. Rev. 42 (2013) 173–201.
[3] Q.Y. Zhang, X.Y. Huang, Prog. Mater. Sci. 55 (2010) 353–427.
[4] B.M. Van der Ende, L. Aarts, A. Meijerink, Adv. Mate. 21 (2009) 3073–3077.
[5] A.M. Srivastava, S.J. Duclos, Chem. Phys. Lett. 275 (1997) 453–456.
[6] Y. Liu, J. Zhang, C. Zhang, J. Jiang, H. Jiang, J. Phys. Chem. C 120 (2016) 2362–2370.
[7] J. Li, J. Sun, J. Liu, X. Li, J. Zhang, Y. Tian, S. Fu, L. Cheng, H. Zhong, H. Xia, B. Chen, Mater. Res. Bull. 48 (2013) 2159–2165.
[8] J.L. Wang, E.H. Song, M. Wu, W.B. Dai, S. Ye, Q.Y. Zhang, Mater. Res. Bull. 74 (2016) 340–345.
[9] Y. Lu, Y. Li, L. Qin, Y. Huang, C. Qin, T. Tsuboi, W. Huang, Mater. Res. Bull. 64 (2015) 425–431.
[10] P.J. Bendall, J. Catlow, P.W.M. Jacobs, J. Solid State Chem. 51 (1988) 159–169.
[11] D.R. Tallent, D.S. Moore, J.C. Wright, J. of Chem. Phys. 67 (1977) 2897–2907.
[12] L. Su, J. Xu, H. Li, W. Yang, Z. Zhao, J. Si, Y. Dong, G. Zhou, Opt. Express 30 (2005) 1003–1006.
[13] D.W. Pack, W.J. Manthey, D.S. McClure, Phys. Rev. B 40 (1989) 9930–9944.
[14] I. Nicoara, M. Stef, Eur. Phys. J. B 85 (2012) 180–186.
[15] A. Guille, A. Pereira, G. Breton, A. Bensalah-ledoux, B. Moine, J. Appl. Phys. 111 (2012) 043104–043108.
[16] Q. Yan, J. Ren, Y. Tong, G. Chen, J. Am. Ceram. Soc. 96 (2013) 1349–1351.
[17] Y. Teng, J. Zhou, X. Liu, S. Ye, J. Qiu, Opt. Express 18 (2010) 9671–9676.
[18] Y. Liu, J. Zhang, C. Zhang, J. Xu, G. Liu, J. Jiang, H. Jiang, Adv. Optical Mater. 3 (2015) 1096–1101.
[19] Y. Liu, C. Zhang, Z. Cheng, Z. Zhou, J. Jiang, H. Jiang, Inorg. Chem. 55 (2016) 8628–8635.
[20] M.Y.A. Yagoub, H.C. Swart, P. Bergman, E. Coetsee, A.I.P Advances 6 (2016) 025204–025215.
[21] F. Wang, Y. Han, C.S. Lim, Y. Lu, J. Wang, J. Xu, H. Chen, C. Zhang, M. Hong, X. Liu, Nature 463 (2010) 1061–1065.
[22] M.Y.A. Yagoub, H.C. Swart, E. Coetsee, J. Lumin. 187 (2017) 96–101.
[23] M.Y.A. Yagoub, H.C. Swart, L.L. Noto, P. Bergman, E. Coetsee, Materials 8 (2015) 2361–2375.
[24] S.M. Kaczmarek, T. Tsuboi, M. Ito, G. Boulon, G. Leniec, J. Phys.: Condens. Matter 17 (2005) 3771–3786.
[25] Y. Ohno, J. Electron Spectrosc. Relat. Phenom. 165 (2008) 1–4.
[26] I. Charkendorff, J., Onsgaard, J. Schmidt-May, R. Nyholm, Surf. Sci. 160 ('985) 587–598.
[27] M.Y.A. Yagoub, H.C. Swart, L.L. Noto, J.H. O'Connell, M.E. Lee, E. Coetsee, J. Lumin. 156 (2014) 150–156.
[28] M.Y.A. Yagoub, H.C. Swart, M.S. Dhlamini, E. Coetsee, Opt. Mater. 60 (2016) 521–525.
[29] W.J. Manthey, Phys. Rev. B 8 (1973) 4086–4098.
[30] Q. Yan, J. Ren, Y. Tong, G. Chen, J. Am. Ceram. Soc. 96 (2013) 1349–1351.
[31] H. Wen, P.A. Tanner, Opt. Mater. 33 (2011) 1602–1606.
[32] B. Fan, C. Point, J.L. Adam, X. Zhang, X. Fan, J. Appl. Phys. 110 (2011) 113107–113114.
[33] S.M. Kaczmarek, T. Tsuboi, M. Ito, G. Boulon, G. Leniec, J. Phys.: Condens. Matter 17 (2005) 3771–3786.
[34] L. Su, J. Xu, H. Li, L. Wen, W. Yang, Z. Zhao, J. Si, Y. Dong, G. Zhou, J. Cryst. Growth 277 (2005) 264–268.